Mechanical Technology and Engineering Insights

www.mtei.reapress.com

Mech. Technol. Eng. Insights. Vol. 2, No. 3 (2025) 222–232.

Paper Type: Original Article

Lattice Boltzmann Simulation of Bubble Dynamics in a Confined Channel

Ramin Goudarzi Karim[1,*], Seyyed Esmaeil Najafi[2]

[1] Department of CIS, Stillman College, Tuscaloosa, Alabama, USA; rkarim@stillman.edu.

[2] Department of Industrial Engineering, Science and Research Branch, Islamic Azad University, 13 Tehran, Iran; enajaf@iaihe.ac.ir.

Citation:

Received: 21 September 2024 *Revised: 17November 2024* *Accepted: 23 January 2025*	Goudarzi Karim, R., & Najafi, S. E. (2025). Lattice Boltzmann simulation of bubble dynamics in a confined channel. *Mechanical Technology and Engineering Insights, 2*(3), 222-232.

Abstract

In this study, a numerical analysis of the buoyancy-driven rise of a single bubble within a confined channel has been carried out by using the Shan-Chen multi-component multiphase Lattice Boltzmann Method (LBM). After verifying the numerical model by comparing results with those predicted by the Laplace law and bubble deformation for a square bubble, a series of numerical simulations has been conducted to explore the effects of the Eötvös number (2-60) and wall effects on bubble dynamics. It has been observed that, with increasing Eötvös number, bubble deformation increases. The bubble shape changes from an elliptical form at a low Eötvös number to a disk-like form at a high Eötvös number. Moreover, at an Eötvös number greater than or equal to 40, shear-induced bubble breakup has been observed. Moreover, streamline analysis shows that, with increasing Eötvös number, the strength of the wake vortex and the level of turbulence both increase. This argument can be explained by the decrease in damping with increasing Eötvös number. For bubbles released close to the wall, an asymmetric shear stress has been observed. This results in an oscillatory trajectory. With an increase in the Eötvös number, the level of oscillation increases. For an Eötvös number between 40 and 60, the oscillatory trajectory results from breakup. It has also been observed that the Morton number (Mo), has a negligible effect on bubble dynamics.

Keywords: Lattice Boltzmann method, Shan-Chen model, Bubble dynamics, Eötvös number, Confined channel, Multiphase flow.

1 | Introduction

Multiphase flows are ubiquitous, and the dynamics of droplets and bubbles is one of the core areas of research in the field of fluid mechanics. Understanding the dynamics of these fluids is vital to the design and optimization of numerous engineering applications, such as liquid-fueled rocket engines, blood pumps, diesel engines, gas turbines, cooling systems, and inkjet printers. In addition, the study of bubble detachment and droplet formation is of great significance for applications such as electronic spray coating and pharmaceutical applications.

Corresponding Author: rkarim@stillman.edu

https://doi.org/10.48313/mtei.v2i3.60

Licensee System Analytics. This article is an open access article distributed under the terms and conditions of the Creative Commons Attribution (CC BY) license (http://creativecommons.org/licenses/by/4.0).

Comprehensive studies on the dynamics of bubbles and droplet deformation were compiled by Clift et al. [1]. The authors primarily presented experimental observations, along with some computational results. Over the last few decades, the Lattice Boltzmann Method (LBM) has been recognized as a promising approach to the simulation of multiphase flows, offering advantages for the complex interfacial dynamics between different phases. Several LBM models have been proposed to simulate multiphase flows. The chromodynamic model, originally proposed by Gunstensen et al. [2] for the simulation of immiscible fluids using the lattice gas method developed by Rothman [3], and later extended by Grunau et al. [4], is one of the earliest models. Later, Swift et al. [5] proposed the free-energy model, where the free-energy concept is incorporated into the LBM.

Among the multiphase Lattice Boltzmann models available, the pseudo-potential model of Shan and Chen [6] has become extremely popular due to its simplicity, flexibility, and ease of implementing force interactions. In the pseudo-potential model, the non-local interactions of the particles are computed based on the additional force applied to the nodes of the lattice. Thus, the pseudo-potential model enables the simulation of phase separation phenomena. An important advantage of the Shan-Chen model is that it allows simulation of different phase viscosity ratios using multiple distribution functions.

Takada et al. [7] used a free-energy model to simulate the motion of buoyancy-driven bubbles and validated the results using the Volume of Fluid (VOF) method. Gupta and Kumar [8] used the Shan-Chen model for simulating the dynamics of single and multiple bubbles under the influence of gravity and buoyancy forces.

Another form of LBM for interface dynamics has been proposed by He, Shan, and Doolen [9]; this model is known as the HSD model. Later, He et al. [10] extended their model for incompressible flows by using two distinct distribution functions to solve for the pressure and velocity fields and to track interface dynamics.

Qin et al. [11] proposed a multi-component multiphase LBM with a Multi-Relaxation Time (MRT) collision operator to investigate bubble breakup in T-shaped microchannels for high density ratios. The findings of this numerical simulation indicate that there are two types of bubble breakup regimes: one due to bubble–wall contact and highlight the significant role of liquid viscosity in accelerating bubble breakup beyond a particular threshold. Chen et al. [12] used a three-dimensional Shan-Chen multi-component LBM to simulate the coalescence of compound droplets with unequal-sized inner cores. Numerical findings of this simulation indicate that there exist discrete processes of liquid bridge growth, relaxation, and breakup/re-coalescence, with inertial scaling of $Rb \propto t1/2$ for the outer liquid bridge. Jing et al. [13] used a modified phase-field LBM coupled with the smoothed boundary method to investigate bubble dynamics in a suspension of obstacles and dendrites in a viscous electrolyte solution. Numerical results from this simulation indicate that wetting of bubble surfaces reduces bubble–obstacle contact, enabling low-deformation sliding. In contrast, wetting of bubble surfaces increases adhesion, resulting in a shear-induced necking instability.

Wan et al. [14] used a phase-field LBM based on the Allen-Cahn equation to simulate bubble dynamics in microchannels with multi-hole orifice plates. Numerical findings of this simulation indicate that there exist two critical Weber numbers, beyond which three bubble dynamics regimes exist, and that increasing contact angles substantially increases bubble passage time, particularly for high Weber number cases. Numerical findings of a numerical simulation by Li et al [15] of bubble dynamics under forced flow in microchannels using a phase-field LBM indicate that bubbles can be detached from a channel wall for high Reynolds numbers, small initial contact angles, and hydrophilic channel walls. Furthermore, bubbles can be split from a bubble resting on a superhydrophilic surface at high Reynolds numbers. Research on multiscale bubble breakup dynamics adjacent to a blade in unsteady turbulence was conducted by Ji et al. [16] using large eddy simulation coupled with the VOF method. Their findings indicated that the dispersion behavior of bubbles in high-velocity-gradient regions surrounding the blade is more pronounced than their ascent behavior, with the bubble fragmentation process governed by the Weber number.

Ding et al. [17] used the LBM coupled with a free-surface approach to study the mechanism of oxygen bubble transport in the porous transport layers and the flow channels of proton exchange membrane water electrolyzers. The results show that hydrophilic porous transport layers favor upward bubble motion over an

optimal range of contact angles. At the same time, fibrous structures are more favorable at high current densities than spherical structures.

A mixed Shan-Chen thermal approach for two-phase Rayleigh-Benard convective heat transfer problems is proposed by Al-Zahiwat et al. [18]. Numerical calculations at relatively high Rayleigh numbers (10^5) show that the convective heat transfer between the hot and cold walls is enhanced by increasing the Rayleigh number. At the same time, the variation of the interface is dependent on the thermal expansion coefficient and the temperature difference.

In the study by Ho and Vu [19], the authors performed numerical calculations of the head-on collision of equal-sized compound droplets, while Zhao et al. [20] extended the calculations to unequal-sized compound droplets. These studies have given detailed insights into the coalescence characteristics and the deformation of compound droplets under different impact conditions.

Despite the achievements, the influence of the boundary on bubble dynamics within the channels remains poorly understood. For example, the interaction between the rising bubble in the channel and the boundary is not well understood, especially in microfluidic systems, enhanced oil recovery, and biomedical applications. Although some studies on the bubble dynamics inside the microchannels with different geometries have been carried out recently [11], [13], [15], the specific influence of the channel walls on the bubble dynamics, such as the trajectory, shape, and breakup inside quiescent fluids, is not yet investigated.

The present study addresses this gap by numerically investigating the buoyancy-driven ascent of a single bubble within a quiescent fluid confined by channel walls. Simulations are performed using the Shan-Chen multiphase LBM framework. A systematic analysis is conducted to evaluate the effects of wall proximity and Eötvös number on bubble deformation, trajectory, and breakup. To the authors' best knowledge, this is the first study to systematically examine the influence of channel walls on bubble dynamics using the LBM approach.

2 | The Lattice Boltzmann Method

The multicomponent-multiphase interparticle potential model was proposed by Shan and Chen in 1993 [6] based on the BGK collision model [21]. In this model, two components (each fluid type corresponds to one component) interact via a force law based on the interparticle potential. The discrete lattice Boltzmann equation for each component is as follows [6]:

$$f_i^{\sigma}(x + e_i\delta_t, t + \delta_t) - f_i^{\sigma}(x, t) = -\frac{1}{\tau^{\sigma}}\left(f_i^{\sigma}(x, t) - f_i^{\sigma(eq)}\left(n^{\sigma}, u_{eq}^{\sigma}\right)\right). \quad (1)$$

The term τ_σ is the relaxation time parameter related to component σ, which is related to the kinematic viscosity as follows:

$$\upsilon^{\sigma} = C_s^2(\tau^{\sigma} - 0.5\delta t). \quad (2)$$

ν^{σ} is the kinematic viscosity of component σ and $C_s^2 = \bar{R}T = \frac{1}{3}$ The equilibrium distribution function of each component is obtained as follows:

$$f_i^{\sigma(eq)} = w_i n^{\sigma}\left[1 + \frac{e_i . u_{eq}^{\sigma}}{c_s^2} + (\frac{e_i . u_{eq}^{\sigma}}{2c_s^4})^2 - \frac{{u_{eq}^{\sigma}}^2}{2c_s^2}\right]. \quad (3)$$

There w_i are weighting coefficients, which are defined as follows:

$$\mathbf{w}_i = \begin{cases} \frac{4}{9}, i = 0. \\ \frac{1}{9}, i = 1-4, \\ \frac{1}{36}, i = 5-8. \end{cases} \quad (4)$$

In this model, c_i represents the lattice velocity in direction i and is expressed as follows:

$$\boldsymbol{c}_i = \begin{cases} (0.0) & i = 0, \\ \left(\cos\left[(i-1)\frac{\pi}{4}\right], \sin\left[(i-1)\frac{\pi}{4}\right]\right).c & i = 1,2,3,4, \\ \left(\cos\left[(i-1)\frac{\pi}{4}\right], \sin\left[(i-1)\frac{\pi}{4}\right]\right)\sqrt{2}.c & i = 5,6,7,8. \end{cases} \quad (5)$$

The number density (n^σ) and the velocity value of component σ (u^σ) at location x and time t are obtained, respectively, as follows:

$$\begin{aligned} n^\sigma(x,t) &= \sum_i f_i{}^\sigma(x,t), \\ n^\sigma u^\sigma(x,t) &= \sum_i e_i f_i{}^\sigma(x,t). \end{aligned} \quad (6)$$

The total interparticle force (forces between two fluids) that is applied to particles of component σ at location x is obtained as follows [22]:

$$F_f^\sigma(x) = F^\sigma(x) = -\psi^\sigma(x) \sum_{\sigma,\bar{\sigma}} G_{\sigma\bar{\sigma}} \sum_i \psi^{\bar{\sigma}}(x + e_i \delta t) e_i. \quad (7)$$

$F_f{}^\sigma$ represents the total force exerted on component σ at location x from fluid particles at neighboring points (interparticle force between two fluids). After the collision step, the new momentum of component σ at each lattice node is modified as follows [22]:

$$\rho^\sigma u_{eq}^\sigma = \rho^\sigma u' + \tau^\sigma F^\sigma. \quad (8)$$

$u^\sigma{}_{eq}$ is the equilibrium velocity of component σ, and F^σ is the total force exerted on component σ. u' is the composite macroscopic velocity, which is very important for analyzing the overall flow. To conserve momentum at each collision step, u' is obtained from the following relation:

$$u' = \frac{\sum_\sigma \rho^\sigma u^\sigma / \tau^\sigma}{\sum_\sigma \rho^\sigma / \tau^\sigma}. \quad (9)$$

The total density, macroscopic momentum, and total pressure at each point of the flow are obtained using the following relation:

$$\begin{aligned} \rho(x,t) &= \sum_\sigma m^\sigma \sum_i f_i^\sigma(x,t), \\ \rho(x,t)U(x,t) &= \sum_\sigma m^\sigma \sum_i e_i f_i^\sigma(x,t) + \frac{1}{2}\sum_\sigma F^\sigma(x,t), \\ P(x,t) &= \bar{R}T \sum_\sigma m^\sigma n^\sigma + \frac{\bar{R}T}{2} \sum_{\sigma\bar{\sigma}} G_{\sigma\bar{\sigma}} \psi^\sigma \psi^{\bar{\sigma}}. \end{aligned} \quad (10)$$

For the total effective force on component σ, we can write:

$$F^{\sigma} = F_f^{\sigma} + F_g^{\sigma} + F_s^{\sigma} + ... \quad (11)$$

In this equation, F^{σ} is the total force applied to component σ, F_f^{σ} is the total force of the interactions of neighboring points between fluids that affects component σ, F_g^{σ} is the gravitational force, and F_s^{σ} is the force that is exerted from the solid surface on component σ, which, in the present paper, due to the negligible effects of the walls on the droplet behavior, is neglected.

3 | Validation of Two-Phase Solution

3.1 | Laplace's Law

Laplace's law expresses the relationship between the pressure inside (Pin) and outside (Pout) of a bubble and the surface tension (σ) between the two fluids. According to Laplace's law, for a two-dimensional bubble, the following relation holds [6]:

$$P_{in} - P_{out} = \frac{\gamma}{R}. \quad (12)$$

A linear correlation is observed between the pressure difference across the bubble boundary and the inverse of the bubble radius. The results show that the simulation accurately represents Laplace's Law. To test the validity of Laplace's Law, static circular bubbles of varying diameters were simulated in an unbounded 2D space of 120x120. The linear regression plot of the pressure difference between inside and outside the bubble, with varying lattice sizes, is shown in Figure. The slope of the plot is 0.19. The surface tension is thus 0.19 for all simulations in this study.

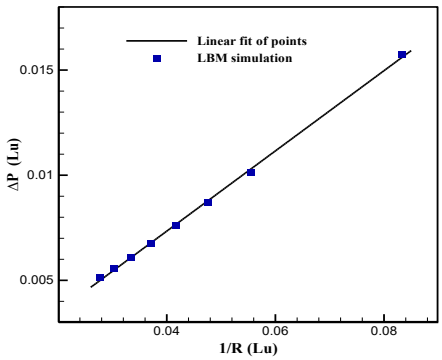

Fig. 1. Demonstration of Laplace's law validation using data points, along with the fitted line.

3.2 | Transformation of a Square Bubble into a Circle

Given that the interface dynamics between the two immiscible fluids is the most complex yet essential aspect of two-phase flow analysis, the validation of the simulation results should be carried out by examining this phenomenon. In this context, the deformation of a two-dimensional square bubble placed in the horizontal plane is presented as a validation example (solution domain size is 120 × 120 lattice units, and the side length of the square bubble is 60 lattice units). Due to interfacial surface tension between the fluids, the bubble evolves to the shape that minimizes its interfacial area, i.e., the energetically favorable shape. As shown in *Fig. 2*, the square bubble deforms into a circular shape in two dimensions. It is a clear indication that the surface tension effects, which form the core of the two-phase flow analysis, are properly modeled.

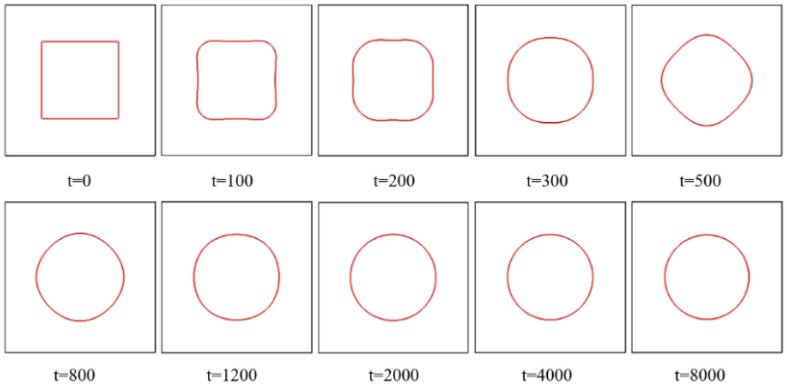

Fig. 2. Deformation of a square droplet released in a horizontal plane at different lattice time steps.

4 | Results and Discussion

In the present simulation, to present the results in a standardized manner, the following dimensionless numbers have been used:

The Eötvös number (Eo), which represents the ratio of gravitational force to surface tension force:

$$\mathrm{Eo}=\frac{g(\rho_d-\rho_c)D^2}{\gamma}. \tag{13}$$

The Morton number (Mo), which actually describes the properties of the fluid surrounding the bubble:

$$\mathrm{Mor}=\frac{g(\rho_c-\rho_d)\rho_c^2\nu_c^4}{\gamma^3}. \tag{14}$$

Dimensionless time:

$$t^*=\frac{t}{\left(\frac{D}{g}\right)^{\frac{1}{2}}}, \tag{15}$$

where g is the gravitational acceleration, ρ_c and ρ_d are the density of the bubble and the density of the fluid surrounding the bubble, respectively, D is the initial diameter of the bubble, γ is the surface tension between the two fluids, υ_d and υ_c are the kinematic viscosity of the bubble and the fluid surrounding the bubble, respectively, and t^* is the lattice time step. In all simulations presented in this paper, the Mo is very small compared to the Eötvös number; therefore, the main determinant of the flow regime is the Eötvös number, and variations in the Mo do not significantly affect the bubble's dynamic behavior.

4.1 | Emergence of a Bubble Along the Channel Symmetry Axis

In all free bubble problems under consideration, the size of the channel is given by 600 × 200, while 50 lattice units give the diameter of the bubble. As the bubble rises, the hydrodynamic pressure exerted on it is greater than that in the central region, resulting in a flattened, elliptical shape, flattened at the poles. The degree of this flattening is directly proportional to the relative magnitude of the hydrodynamic pressure forces to the surface tension effects, the latter of which tends to keep the bubble profile circular. Based on the data in Fig. 3, at low Eötvös numbers, the bubble is not significantly flattened (Eo = 2, Eo = 5). When the values of the Eötvös number are moderate, the bubble is flattened significantly (Eo = 10); at the beginning, the shape evolves similarly to the previous bubble, while later on, the bubble's posterior part becomes convex, eventually resulting in the bubble having the shape of a disk and moving towards the steady-state position. When the

Eötvös number is high (Eo = 20, 30), the bubble is significantly flattened at the beginning. Later, the bubble's restabilization into a disk shape becomes difficult due to its inertia, while the concavity at the bottom of the bubble is retained. When the Eötvös number exceeds 30, the bubble undergoes a transition, during which state changes are observed. In these cases, the bubble's deformation is significant, resulting in a substantial increase in the hydrodynamic pressure acting on the bubble. At the same time, surface tension effects are no longer important, leading to the bubble's breakup into two parts, a phenomenon known as shear-induced breakup.

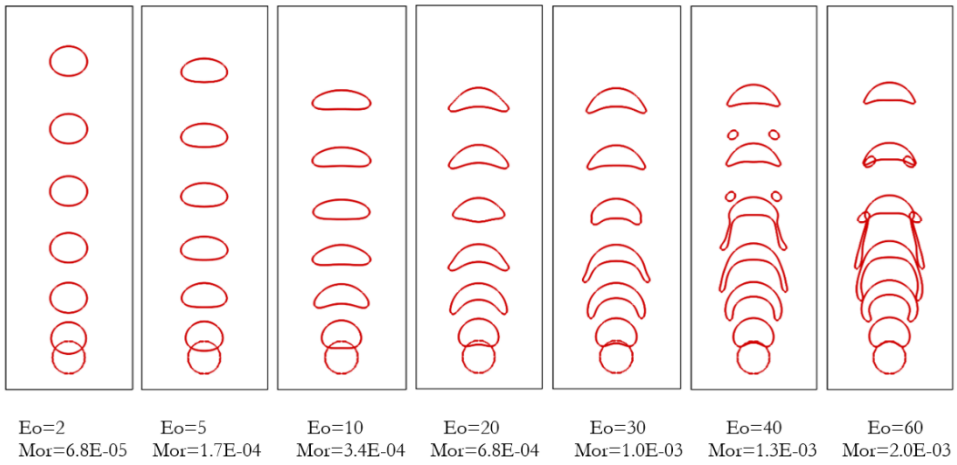

Fig. 3. Evolution of bubble shape along the channel symmetry axis across varying Eötvös numbers (Eo).

4.2 | Effect of Eötvös Number on Streamlines

Fig. 4 illustrates the streamlines of a rising bubble in a fluid for three different Eötvös numbers, each with a distinct characteristic. All of these cases correspond to a dimensionless time of 6. In the case where the Eötvös number is 2 (denoted by case a), the flow remains completely laminar, with vortices confined to the bubble. As the Eötvös number increases, a vortex forms at the bubble's bottom, known as the bubble wake, which results in a turbulent flow field. With a further increase in the Eötvös number, the wakes in the bubble contain larger vortices, leading to a more turbulent flow field. Thus, with an increase in the Eötvös number, resulting in greater bubble inertia, the damping effects of the fluid's viscosity decrease, and turbulence increases in the flow field.

4.3 | Rising of a Bubble from Near One of the Channel Walls

From *Fig. 5* above, it can be observed that, as the bubble starts close to any of the channel walls, shear stresses at the wall cause deformation and rotation. Wall repulsion effects cause the bubble to move towards the channel's vertical symmetry axis. At a low Eötvös number (Eo = 2), the bubble moves towards the vertical symmetry axis. Due to strong surface tension effects and, therefore, a large damping compared to inertial effects (buoyancy), the bubble does not exhibit any oscillation and moves in a straight line along the vertical axis. From *Fig. 5* above, as the Eötvös number increases, a bubble movement phenomenon occurs: as the bubble approaches the vertical symmetry axis, pressure and rotational forces within the bubble cause it to move back. Subsequently, as the bubble approaches the channel wall, wall repulsion and bubble rotational force cause it to move towards the channel's centerline. This phenomenon results in an oscillatory path for the bubble. At very high values of the Eötvös number, i.e., Eo = 40 and Eo = 60, besides an oscillatory path, the bubble also exhibits shear-induced breakup.

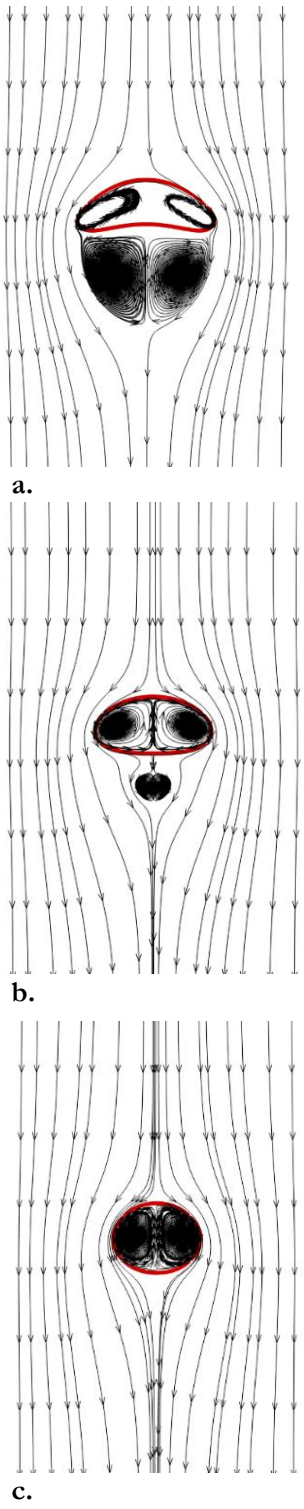

Fig. 4. Display of streamlines around the bubble at different Eötvös and Morton numbers at a dimensionless time of; a. Eo=20, Mo=6.83E-05, b Eo=5, Mo=1.70E-04, and c. Eo=10, Mo=3.41E-04 6.

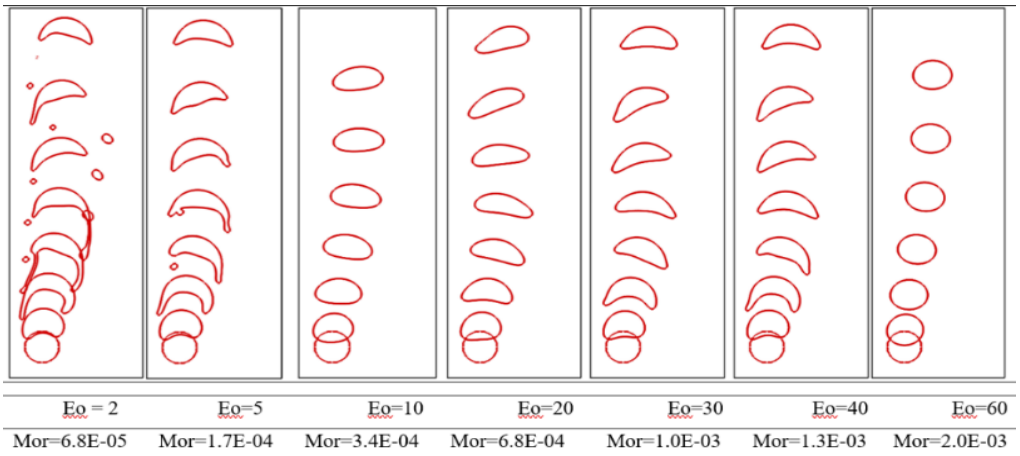

Fig. 5. Display of bubble rising from near the left channel wall at different Eötvös and Morton numbers.

5 | Conclusion

The dynamic behavior of a buoyancy-driven bubble rising in a confined channel has been numerically simulated using the Shan-Chen LBM. The important findings of the simulation are as follows:

I. The bubble deformation is found to increase with the Eo number: at low Eo numbers, the bubble is slightly flattened into an ellipse; at higher Eo numbers, it becomes a disk; and at very high Eo numbers, it breaks up.

II. The flow pattern also changes with the Eo number: at low Eo numbers, the flow is laminar with trapped vortices; at higher Eo numbers, wake vortices and turbulent flow outside the wake occur due to the lack of viscous damping.

III. The proximity of the bubble to the channel wall also leads to an oscillatory path, with bubbles released near the wall exhibiting oscillations towards and away from the wall, and the oscillation amplitude increases with the Eo number.

IV. There is also a critical Eo beyond which the bubble breaks up, irrespective of proximity to the wall, with a range of 30-40.

V. The influence of the Mo is found to be negligible, as it is much smaller than the Eo number in all cases.

The Shan-Chen LBM has shown promise for simulating the complex behavior of buoyancy-driven bubbles in confined channels, and the results will be useful for developing microfluidic devices.

Conflict of Interest

The authors declare no conflict of interest.

Data Availability

All data are included in the text.

Funding

This research received no specific grant from funding agencies in the public, commercial, or not-for-profit sectors.

References

[1] Clift, R., Grace, J. R., & Weber, M. E. (2005). Bubbles, drops, and particles. https://www.researchgate.net/publication/233845152_Bubbles_Drops_and_Particles

[2] Gunstensen, A. K., Rothman, D. H., Zaleski, S., & Zanetti, G. (1991). Lattice Boltzmann model of immiscible fluids. *Physical review a*, *43*(8), 4320. https://doi.org/10.1103/PhysRevA.43.4320

[3] Rothman, D. H., & Keller, J. M. (1988). Immiscible cellular-automaton fluids. *Journal of statistical physics*, *52*(3), 1119–1127. https://doi.org/10.1007/BF01019743

[4] Grunau, D., Chen, S., & Eggert, K. (1993). A lattice Boltzmann model for multiphase fluid flows. *Physics of fluids a: fluid dynamics*, *5*(10), 2557–2562. https://doi.org/10.1063/1.858769

[5] Swift, M. R., Osborn, W. R., & Yeomans, J. M. (1995). Lattice Boltzmann simulation of nonideal fluids. *Physical review letters*, *75*(5), 830. https://doi.org/10.1103/PhysRevLett.75.830

[6] Shan, X., & Chen, H. (1993). Lattice Boltzmann model for simulating flows with multiple phases and components. *Physical review e*, *47*(3), 1815. https://doi.org/10.1103/PhysRevE.47.1815

[7] Takada, N., Misawa, M., Tomiyama, A., & Hosokawa, S. (2001). Simulation of bubble motion under gravity by lattice Boltzmann method. *Journal of nuclear science and technology*, *38*(5), 330–341. https://doi.org/10.1080/18811248.2001.9715037

[8] Gupta, A., & Kumar, R. (2007). Lattice boltzmann simulation to study multiple bubble dynamics. *ASME international mechanical engineering congress and exposition*. ASME. (Vol. 43025, pp. 1593–1604). https://doi.org/10.1115/IMECE2007-43218

[9] He, X., Shan, X., & Doolen, G. D. (1998). Discrete Boltzmann equation model for nonideal gases. *Physical review e*, *57*(1), R13. https://doi.org/10.1103/PhysRevE.57.R13

[10] He, X., Chen, S., & Zhang, R. (1999). A lattice Boltzmann scheme for incompressible multiphase flow and its application in simulation of Rayleigh--Taylor instability. *Journal of computational physics*, *152*(2), 642–663. https://doi.org/10.1006/jcph.1999.6257

[11] Qin, M., Zhang, N., Zhang, H., Zhang, W., Liu, P., Wang, M., … & Dong, J. (2025). LBM simulation of bubble breakup dynamics in microchannels at large density ratios. *Chemical engineering science*, *306*, 121253. https://doi.org/10.1016/j.ces.2025.121253

[12] Chen, H. (2025). Coalescence of compound droplets with unequal-sized inner cores. *AIChE journal*, e70164. https://doi.org/10.1002/aic.70164

[13] Jing, H., Xing, H., Du, X., Sun, D., Zheng, Y., & Han, Y. (2025). Bubble rising dynamics with obstacles and dendrite in viscous electrolytes: A smoothed boundary method reformulated phase-field lattice-Boltzmann study. *Physics of fluids*, *37*(8). https://doi.org/10.1063/5.0281871

[14] Wan, J., Ding, H., Wang, N., Dong, W., & Wang, Z. (2025). LBM simulation of bubble dynamics in a microchannel with multi-hole orifice plate. *European journal of mechanics-b/fluids*, *113*, 204260. https://doi.org/10.1016/j.euromechflu.2025.204260

[15] Li, D., Xing, J., Zhang, Z., & Wang, H. (2025). Numerical investigation on the dynamic behavior of bubbles under forced flow in a microchannel. *RSC advances*, *15*(29), 23414–23426. https://doi.org/10.1039/d5ra02116b

[16] Ji, J., Li, C., Xie, J., & Tang, Z. (2025). Multiscale bubble breakup dynamics adjacent to a blade in unsteady turbulence within a bubble breaker. *Physics of fluids*, *37*(1). https://doi.org/10.1063/5.0249730

[17] Ding, Z., Li, R., & Luo, K. H. (2025). LBM studies on oxygen bubble transport in porous transport layers and flow channel of proton exchange membrane water electrolyzers. *Journal of power sources*, *642*, 236959. https://doi.org/10.1016/j.jpowsour.2025.236959

[18] Al-Zahiwat, M. M., Omar, I., Babadoust, S., Sabri, L. S., Yazdkhsti, A., Sajadi, S. M., … & Emami, N. (2025). Using of multi-phase thermal model of the lattice boltzmann method for simulation of two-phase rayleigh--Bénard convective heat transfer. *Results in chemistry*, *13*, 101975. https://doi.org/10.1016/j.rechem.2024.101975

[19] Ho, N. X., & Vu, T. V. (2023). Numerical study of head-on collision of two equal-sized compound droplets. *Physics of fluids*, *35*(6). https://doi.org/10.1063/5.0153227

[20] Zhao, Y., Wang, Z., Yang, Q., Zhang, B., Gao, Q., & Hong, S. (2025). Kinetic study of head-on collisions of unequal-sized compound droplets. *Physics of fluids*, *37*(1). https://doi.org/10.1063/5.0246229

[21] Bhatnagar, P. L., Gross, E. P., & Krook, M. (1954). A model for collision processes in gases. I. Small amplitude processes in charged and neutral one-component systems. *Physical review*, *94*(3), 511. https://doi.org/10.1103/PhysRev.94.511

[22] Shan, X., & Doolen, G. (1995). Multicomponent lattice-Boltzmann model with interparticle interaction. *Journal of statistical physics*, *81*(1), 379–393. https://doi.org/10.1007/BF02179985